Polymer Testing 108 (2022) 107499

Contents lists available at ScienceDirect

Polymer Testing

journal homepage: www.elsevier.com/locate/polytest

3D printing and post-curing optimization of photopolymerized structures: Basic concepts and effective tools for improved thermomechanical properties

Martina Šťaffová [a], František Ondreáš [a,b], Juraj Svatík [a], Marek Zbončák [c], Josef Jančář [a], Petr Lepcio [a,*]

[a] Central European Institute of Technology, Brno University of Technology, Purkyňova 123a, 612 00, Brno, Czech Republic
[b] Contipro a.s., Dolni Dobrouc 401, 56102, Dolni Dobrouc, Czech Republic
[c] Prusa Polymers a.s., Partyzánska 188/7a, 170 00, Praha, Czech Republic

ARTICLE INFO

Keywords:
3D printing
Masked stereolithography
Post processing
DMA
Print orientation
Network density

ABSTRACT

The final thermo-mechanical properties of structural parts fabricated by masked stereolithography (MSLA) are highly determined not only by the processing parameters, but also by the post-processing methods. Improper implementation of post-treatment often leads to underperforming printouts. A novel tool for complex characterization of 3D printed bodies was developed and systematically demonstrated on a commercial free-radical photopolymerization (FRP) resin. The method relies on superimposed static and oscillatory mechanical test combining the heat deflection temperature (HDT) measurement together with the dynamic mechanical analysis (DMA) in a single test for fast and reliable characterization of parameters determining the curing behaviour of the photopolymer. The influence of post-curing time was addressed with a special focus on network density. Furthermore, the print orientation, having a high impact on mechanical properties, is discussed with a particular regard on the residual stress mitigation in future applications, such as 3D-printed cellular bodies.

1. Introduction

3D printing, also known as additive manufacturing (AM) has experienced a rapid growth in recent decades. Freedom of design, customization, waste reduction, fast prototyping, high precision, avoiding the use of tools and ability to manufacture complex structures are the main benefits of 3D printing [1]. The main disadvantage is the heterogeneity of the 3D printed bodies due to the defects between the adjacent print layers or voxels or inhomogeneous conversion of the monomer throughout the printouts. In general, the parts 3D printed by various techniques often fall behind the bulk processed materials in mechanical properties unless the print layers/voxels are properly fused together [2,3]. Furthermore, the heterogeneous character makes the overall mechanical performance sensitive to the print orientation which determines the distribution of defects [4]. On the other hand, smart designs could engineer weak spots on purpose to modify the overall mechanical performance. Even though the ultimate strength is reduced, a local failure at these weak spots could prevent a catastrophic fracture in brittle materials [5].

Recent developments have reduced the cost of 3D printers, enabling desktop fabrication of 3D objects even at home, thereby expanding its application field from science and industry to small businesses and general public. Among the 3D techniques, stereolithography (SLA) is the earliest method patented in 1986 by Hull [6] and also the first commercially employed one. It has been reported that almost 50% of the 3D printing market can be attributed to photopolymers [7]. Photopolymers have been used in fields such as lightweight engineering [8], ultrasonic sensing [9] or functional constructs [10]. While they have yet to be approved for long-term surgical implantation, they have been used in medical device applications [11] such as hearing aids, microneedles [12] or drug-loaded scaffolds with controlled release properties [13]. However, there are still numerous issues that need to be addressed in order to full scale the SLA 3D printing. Moreover, due to the layered manufacturing process, the products tend to be anisotropic, with the boundary between layers representing weak regions with maximum residual stresses [14].

The traditional SLA technique employs an irradiation with a controlled ultraviolet (UV) spotlight or laser to polymerize the liquid

* Corresponding author. Postal address: CEITEC VUT, Purkynova 123a, 612 00, Brno, Czech Republic.
E-mail addresses: martina.staffova@ceitec.vutbr.cz (M. Šťaffová), petr.lepcio@ceitec.vutbr.cz (P. Lepcio).

https://doi.org/10.1016/j.polymertesting.2022.107499
Received 22 December 2021; Received in revised form 20 January 2022; Accepted 2 February 2022
Available online 4 February 2022

resin point by point, which results in a patterned layer of the crosslinked polymer [15]. Masked stereolithography (MSLA) was derived from the SLA technique by putting a mask with a controlled shape between the light source and the resin tank to cure a specific 2D pattern. These methods exhibit higher build speed, excellent surface quality and precision with a typical feature resolution of tens to hundreds of micrometers depending on the technological parameters (light source, wavelength, pixel size, material, etc.). The typical curing behaviour of common free radical polymerization resins is characterized by a high built speed of a polymer network (high-reactivity), fast transition from liquid to solid (gelation) and a quick setting of the final mechanical properties (curing), which leads to increased stiffness as a result of changes on molecular level of the photopolymer material [16,17]. A crosslinking of the system with higher functional acrylate oligomers and monomers is necessary in order to increase the network density and thus the thermomechanical stability suitable for the 3D printing process [18].

Numerous research activities on kinetics and characterization of photopolymers have been performed [19–22]. Hong et al. conducted research on mechanical properties of UV-curable 3D printing materials, along with their anisotropic and size dependent behaviour [23]. The anisotropic properties were clearly seen in tensile toughness and elongation at break with respect to a printing direction, while it was not observed in their Young's modulus and tensile strength. Kotlinski performed an in-depth analysis of commercial AM materials with respect to their mechanical properties, including guideline for design engineers [24]. The diffusion-controlled kinetics of curable 3D printing materials has been studied by Kim et al. [25] and kinetic model was developed to describe the limited conversion of cure as a function of isothermal curing temperatures. Gao et al. [26] presented photopolymerization kinetic model to predict printing effects, while it was concluded that printing settings had a great influence on printing quality for paradoxical relationship between print speed and resolution. By Hofstetter et al. the cure degree of a cured layer was evaluated in order to find a way to characterize photopolymers [16] concluding that with the combination of Jacobs working curve (cure depth), the mechanical properties and double bond conversion (DBC) from the photorheometer (cure degree), it is possible to completely characterize the curing behaviour of photopolymers. Further the great effect of post-curing and solvent post-processing methods on mechanical properties have been studied [27,28]. However, there is still need for better understanding of the photopolymerization process as well as for utilized characterization methods of novel resins.

Herein, we present a novel approach to characterize the thermomechanical properties, which shall deliver a powerful tool for future excessive studies of photocurable 3D printing resins and their use in engineering applications. We present an effective, reliable, time saving, and relatively simple hybrid method combining the DMA and HDT measurements into a single test. The advantages in comparison to conventional methods of HDT and DMA measurements methods are lower material consumption, time, effort, and capacity savings due to faster sample preparation and measurement, and collection of additional data in a single run compared to situation where only one test is carried out. Furthermore, it lowers the equipment requirements, if only one instrument is needed instead of two. It originated from the fundamental investigation of polymer glass dynamics via superimposed small static stress typical for HDT measurement and oscillatory deformation employed by the DMA [29]. The thermomechanical properties were studied with a representative commercial free radical polymerization (FRP) photo-resin. The parameters monitored in this study were the curing time, specimen thickness and orientation on the print platform. The presented hybrid method showed a great sensitivity to all these parameters and correlated them to the network density, a key structural parameter established by this technique which directly depends not only on the resin composition and the photochemical reaction upon the 3D printing, but also on the subsequent processing steps. The results will help improve the understanding of the photopolymerization and MSLA technique for engineers and scientists as well as for the rapidly growing small business, and general public community.

2. Material and methods

2.1. Materials

A commercial UV curable acrylate-based transparent clear resin (CR) obtained from Shenzhen Yongchanghe Technology Co., Ltd. was used as obtained. According to its UV-VIS spectra recorded by Jasco V-730 UV-VIS spectrophotometer and compared to the neat TPO (RAHN, Switzerland) dissolved in acetonitrile (Fig. S1), the resin contained 6% of the diphenyl (2,4,6-trimethylbenzoyl)-phosphine oxide (TPO) free radical photoinitiator. This resin was selected as a representative of many common commercial photocurable resins, either for non-demanding applications or for prototyping, which have similar chemistry, penetration depth and critical energy. Further thermo-mechanical properties of the material are assessed below.

2.2. MSLA 3D printing

Samples were 3D printed with Prusa SL1 printer (Prusa Research, Czech Republic), based on the Mask Stereolithography technology (MSLA). The irradiation intensity of the 3D printer was 0.661 mW cm^{-2}, measured at the surface of the FEP foil in the vat with the Flame-S-UV-VIS-ES spectrometer (Ocean Insight, USA). The maximum light intensity was found at 405 nm (Fig. S1). Standard FEP foil with thickness of 150 μm was used. The exposure time was selected according to the Jacobs working curves as described further in text. All specimens were printed with the exposure time of the initial layer of 15 s. Further layers were printed with the exposure time of 10 s. The layer thickness was set to 50 μm. If not specified otherwise, the samples were printed in *x* direction, i.e., with the narrower face aligned to the built platform plane. Printed specimens were washed in isopropanol for the shortest possible time (less than 15 s) to avoid monomer extraction, swelling, and the consequent deterioration of the mechanical properties [27,30,31]. It was observed that the exposure time of the fresh printout to the cleaning in isopropanol had a significant influence on sample appearance and the presence of defects. A significant effect on thermomechanical properties and final application performance can be expected. Thus, all samples were cleaned for less than 15 s in this study. Nevertheless, the effect of solvent washing on the post-treatment was beyond the scope of the current study even though it is of great importance. Post processing was performed with the Prusa CW1 curing and washing unit with approx. irradiation intensity of 10 mW cm^{-2}. The samples were dried and cured at 35 °C. The influence of sample thickness, the curing time, print orientation and position of the sample on the printing stage on thermomechanical performance was studied. All specimens were printed off-centered, to provide the most uniform light distribution on the printing plate.

2.3. Thermomechanical properties analysis

A method for simultaneous DMA and HDT analysis was performed with RSA G2 from TA Instruments to establish material constants and printing parameters. The stiffness measured through the dynamic oscillatory deformation represented by storage modulus *G'* of the studied materials was evaluated at different temperatures and the glass transition temperature T_g was determined from the maximum of the loss factor (tan δ). Furthermore, HDT measurement was based on the ASTM D 648-07 Standard Test Method for Deflection Temperature of Plastics Under Flexural Load in the Edgewise position. The size of the test specimens was proportionally reduced against the standard body to 48.5 × 5 x 2–5 mm^3. The specimens were loaded in three-point bending setup with 40 mm distance between supports in the edgewise direction. HDT was determined at a deformation that corresponded to a deflection

of 0.25 mm of the normalized body, which equals to 0.195% flexural strain for the samples used. The flexural strain was calculated according to equation (1):

$$\varepsilon_f = \frac{600 \cdot s \cdot h}{L^2} \quad (1)$$

Where s is the deflection, h is thickness and L is the span. The frequency of oscillating deformation was set to 1 Hz and the strain amplitude was 0.002%. The imposed stress of 0.455 MPa was applied by the upper geometry and the heating from 30 to 160 °C at the rate of 2 °C/min was mediated by hot air. The validity of this presented method is discussed in more detail in the results section. Moreover, the results were correlated to the hardness which was measured with a handheld Shore D durometer (SMT, Netherlands) with a 30° cone, radius of 0.1 mm and the maximum force of 44.5 N, a fast, cheap, and simple technique which is available not only to specialized laboratories, but could be easily adopted also by small business and hobby users.

2.4. Photopolymerization assessment

The photopolymerization reaction was assessed by photo-DSC and photo-rheology using DSC Discovery and ARES G2, respectively, both from TA Instruments. The uncured resin loaded in the instruments was illuminated by a constant 405 nm LED light source with a power intensity of 0.661 mW cm^{-2} measured inside the instrument at the sample location, i.e., matching the power density of the SL1 printer. The onset of illumination was set to the time of 0 s. Photo-DSC was performed in an open aluminium pan with 15.0 μl of sample at a constant temperature of 25 °C against an empty reference pan which was also illuminated by the same light. The results were compared to high intensity curing using the same photo-calorimetric setup and the OmniCure S2000 curing unit equipped with a 200 W high pressure mercury vapor UV lamp with a power density of 30 W cm^{-2}. Photo-rheology was conducted under ambient conditions in steady oscillation at frequency of 4 Hz, strain amplitude of 2%, and gap of 100 μm. A special disposable UV-curing plate-plate geometry (transparent acrylic upper geometry, aluminium lower geometry) with a diameter of 25 mm was used to illuminate the top surface of the sample.

The samples for the cure depth (C_d) measurement were printed using the SL1 printer (Prusa Research, Czech Republic). The resin was poured into the printer's vat and a single layer square shape was photopolymerized in the absence of the printing platform. The cure depth of the layer was measured with a micrometre as a function of the exposure energy by varying the exposure time. Jacobs working curve was created as a linear-logarithmic plot of cure depth dependence on the exposure energy (E_{max}). The intersection of the working curve with the x-axis gives the critical exposure E_c, e.g., the exposure at which the resin solidification starts to occur. The slope of logarithmic-linear plot represents the penetration depth (D_p) of light into a resin at which the irradiation dose E_z equals to the E_{max}/e *where* e is the Euler's number (see Eq. (2)). Through the application of the Beer-Lambert law, the theoretical relation between the resin characteristics and exposure can be developed (see Eq. (3)) [32].

$$C_d = D_p \cdot ln\left(\frac{E_{max}}{E_c}\right) = D_p \cdot ln\, E_{max} - D_p \cdot ln\, E_c \quad (2)$$

$$E_z = E_{max} \cdot exp\left(-\frac{z}{D_p}\right) \quad (3)$$

When Eq. (2) is fitted with a simple logarithmic function $y = a \ln x + b$, where the x and y represent the exposure energy and the cure depth, respectively, the penetration depth is directly equal to the parameter a while the critical exposure could be evaluated as (Eq. (4)):

$$E_c = e^{-\frac{b}{a}} \quad (4)$$

All samples were printed as squares with the dimension of (10 × 10) mm^2, while the curing time varied between 10 and 60 s. After printing, the squares were cleaned with isopropanol and their thickness was measured (minimum five times per each sample).

2.5. FTIR measurement of double bond conversion

In order to find out the conversion ratio variation throughout the sample's thickness, the FTIR measurement was taken with VERTEX 70v FTIR equipped with Hyperion 3000 Microscope in ATR mode. The specimen was printed with dimensions of 48.5 × 5 × 5 mm^3 and post-cured for 1 min with the Original Prusa CW1 curing machine. The sample was cryofractured in liquid nitrogen to expose the bulk body and measured at eleven evenly distributed spots along the thickness of the broken plane.

2.6. Structural observation

The surface structure of the printed specimens was investigated with the Confocal Laser Scanning Microscope Olympus Lext OLS4100 equipped with a 405 nm laser. The SEM observation was performed on cryo-fractured samples coated with a 10 nm sputtered gold (ACE 600, Leica) with a Mira 3 XMU microscope (Tescan, Czech Republic) in low-vacuum mode at 10 kV acceleration voltage using the LVSTD secondary electron detector designed for low vacuum operation and observation of organic low conductive samples.

3. Results and discussion

The chemical composition, functionality, interactions, stiffness, and chain length of the monomers strongly affect the photopolymerization reaction, safety, and other properties of the final systems. Thus, it is of great importance to have a reliable testing method for characterizing these materials. Thermomechanical properties directly reflect the structure of the analysed system. Therefore, they represent a suitable tool for evaluating the influence of the processing and post-processing parameters on the photopolymerized 3D printed systems.

The network density (υ_e) could be directly determined by dynamic mechanic analysis (DMA) through measuring the modulus at a temperature well above the T_g, in the rubbery region. The network density ν_e is estimated from the rubbery modulus using the theory of rubber elasticity (Eq. (5)) [33,34]:

$$\nu_e = 2(1+\upsilon)\frac{G_N^0}{RT}, \quad (5)$$

where υ is the Poisson's ratio, R is the gas constant, T is the temperature, and G_N^0 is the rubber-plateau modulus. The network densities were calculated assuming the material is incompressible (υ = ½), using the rubber-plateau modulus G_N^0 determined at the fixed temperature of 135 °C. Furthermore, the stiffness represented by storage modulus E' of the studied materials could be evaluated at different temperatures, while the glass transition temperature T_g, at which the segmental motion of polymer chains is released and the stiffness decreases significantly, was determined from the maximum of loss factor (tan δ).

Another common tool for evaluating the thermomechanical properties is the maximum deformation (D_{max}) and the heat deflection temperature (HDT) which indicates the temperature at which the body bends at a given deflection under the constant load. These parameters are also directly related to the structure of the analysed system. We have adopted the HDT measurement based on the ASTM D 648-07 Standard Test Method for Deflection Temperature of Plastics Under Flexural Load in the Edgewise position, proportionally reducing the size specified for the normalized specimens to 48.5 × 5 x 2–5 mm^3. The static stress was maintained at 0.455 MPa.

In order to save time and material, a combined DMA and HDT

measurement was developed which was performed on RSA G2 (TA Instruments, USA). This method, originating from the fundamental investigation of the polymer glass dynamics [29], superimposes the small static stress used by the HDT measurement with the oscillatory stress of the DMA method to establish the material constants and processing parameters in a single run (Fig. 1). The hybrid method is particularly convenient for characterizing 3D printed materials because of the rather long processing times and often the limited build volume. Nevertheless, this method is only eligible to test solid specimens. Thus, firstly are presented the results on photocuring assessment obtained by other techniques which were used to obtain the basic printing parameters. Further continue the discussion of the mechanical properties and network density.

The glassy region at low temperatures was characterized with a relatively weak dependence of the storage modulus on the temperature and low tan δ values (Fig. 1). As the heating continued, a drop in storage modulus and peak of tan δ appeared for all samples, marking the glass transition region where the material losses its stiffness. The rubbery behaviour with its characteristic rubbery plateau of storage modulus and low tan δ values followed at even higher temperatures. The terminal zone and macroscopic flow of the samples was not observed due to their highly crosslinked structure. However, failure of the samples at specific temperature associated with the printing direction was observed which is described further in the text.

3.1. Photocuring assessment

The parameters of the photocuring process were evaluated using the Jacobs working curves, photo-DSC and photo-rheology to properly adjust the printing parameters. The Jacobs working curve of the tested resin is shown in Fig. 2. The critical exposure (E_c) and penetration depth (D_p) were calculated according to equations (3) and (4). The resin showed a typical curing behaviour for acrylate photopolymers, which can be characterized by high reactivity and fast gelation and curing. The penetration depth must be larger than the printing layer thickness in order to ensure sufficient adhesion between the layers and avoid delamination [35]. Furthermore, the Jacobs working curve revealed a sudden increase in the cure depth rate at about 9.6 mJ cm^{-2} (~14.5 s). The data beyond this critical point could be fitted with an independent logarithmic fit which yielded higher D_p as well as the E_c compared to the initial photopolymerization reaction. The process behind this sudden change in the curing behaviour could be better understood from the photo-DSC and photo-rheological results which discussion follows.

The photo-DSC revealed two exothermic peaks when the resin was

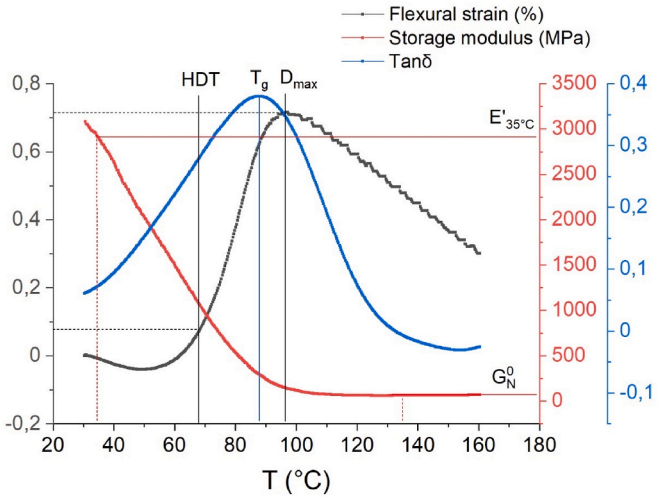

Fig. 1. Graph showing main values read from the developed technique combining DMA and HDT measurement of photo-resins. (color in print)

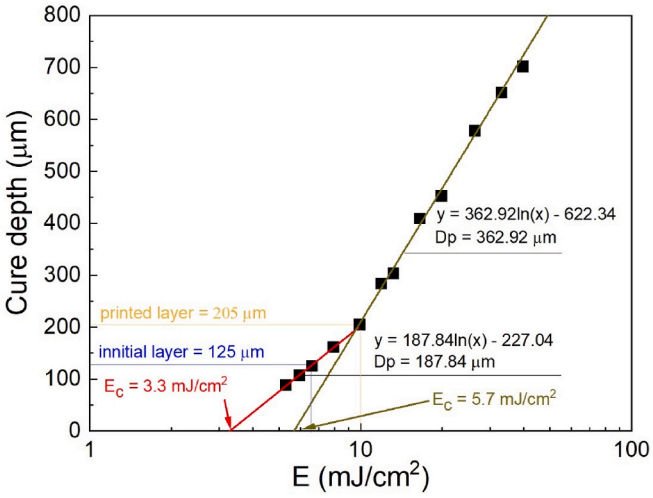

Fig. 2. Jacobs working curve for the tested resin. Standard deviation is below 8 μm for all samples and therefor is not visible in the graph.

illuminated with low intensity (0.661 mW cm^{-2}) blue LED light (405 nm) with the maximum conversion rate reached at (12.3 ± 0.3) mJ·cm^{-2} (~18.6 s) followed by another local maximum at (213.6 ± 19.5) mJ·cm^{-2} (~323.1 s) (Fig. 3 left). The second peak is reportedly connected to the reaction of the heavier monomer (or oligomer) in a mixture containing at least two monomers with different molecular weight [36]. We note that the second peak is not commonly observed in photo-DSC results when a high intensity (30 W cm^{-2}) wide-range UV spectrum mercury lamp is used for the curing (Fig. 3 right). Interestingly, the threshold energy of 9.6 mJ cm^{-2} at which the cure depth started to grow faster (Fig. 2) slightly preceded the maximum of the first peak (Fig. 3 left) but it is obvious that much higher exposure doses are required to fully cure the resin. The total curing enthalpy was established to (−343.8 ± 4.1) J·g^{-1}. We point out that the maximum conversion rate took place at varying time depending on the volume of the cured sample (data shown for 15.0 μl). In the contrary, the total curing enthalpy was quite insensitive to this parameter but that would not be expected unless for very thick samples.

The photo-rheology (Fig. 4) revealed that the gel point evaluated at the crossover of storage G' and loss G'' moduli took place at 3.0 mJ cm^{-2} (~4.6 s), corresponding well to the critical energy of 3.3 mJ cm^{-2} established by the Jacobs working curves. At higher exposure doses, the increase of G' has saturated, accompanied with a slight overshoot at G" and a peak at the tan δ at 7.1 mJ cm^{-2} (~10.8 s). This may possibly relate to the vitrification point, i.e., the moment when the system turned into glassy state. That happens when the gradually increasing T_g of the cured system exceeds the experimental temperature at which the curing/measurement takes place. The detailed evaluation of T_g in the printed bodies will be discussed later. Interestingly, the sudden drop in the curing heat flow at 12.3 mJ cm^{-2} (Fig. 4 left) took place 7.8 s after the vitrification point (Fig. 4 right). The transition to glass region would be expected to slow down the diffusion of species within the sample and hinder the propagation of the ongoing reaction, but this phenomenon may also possibly relate to the full consumption of the lighter monomer. The curing energy of 5.7 mJ cm^{-2} (~8.6 s) required to polymerize a 100 μm layer (Fig. 2), i.e., to span across the gap used for the rheological measurements, is lower than the energy required for the vitrification to occur. Instead, it correlates with the exposure dose at which the rapid growth of G' and G" is replaced by nearly indistinct change in properties (Fig. 4 right). We note that the plate-plate geometry setup of the photo-rheometer may struggle to transfer the stress into very stiff samples, rendering the procedure insensitive to further structural changes beyond this point.

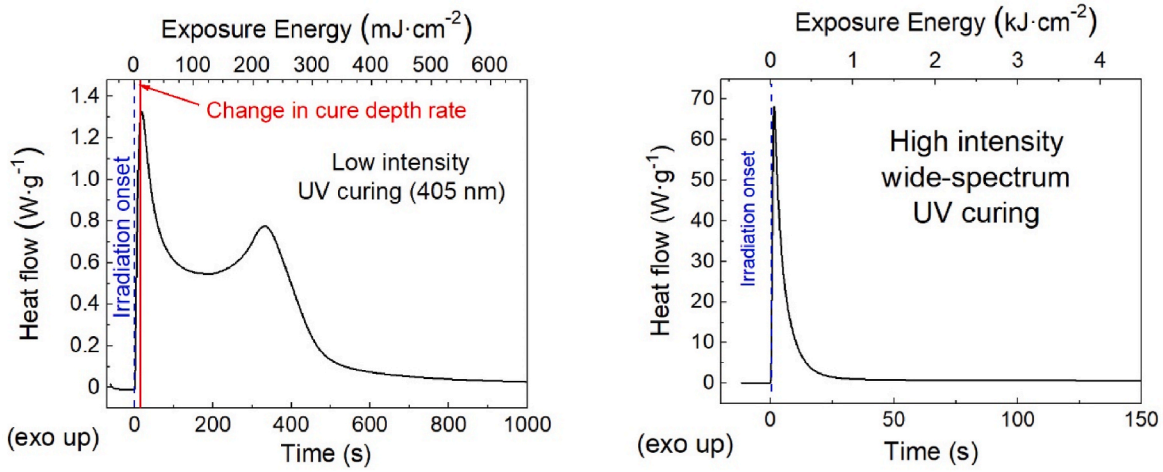

Fig. 3. Normalized heat flow recorded by a photo-DSC as a function of exposure time and exposure energy upon irradiation by the low intensity 405 nm UV LEDs (left) and high intensity wide-spectrum mercury lamp (right).

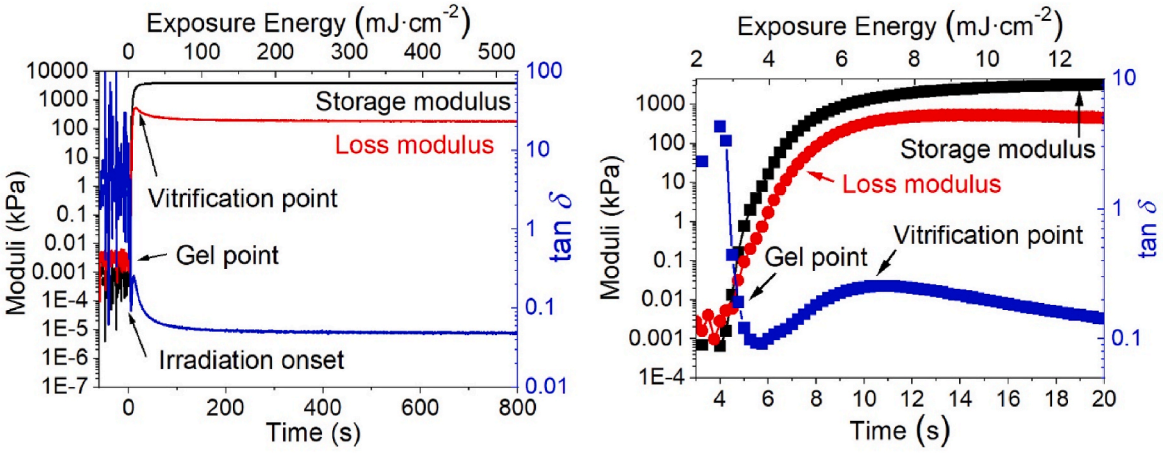

Fig. 4. Photorheological assessment of the UV curing process – dependence of storage (black) and loss (red) moduli and loss factor tan δ (blue) on the exposure time and exposure energy (left) with the detail of the gel point and vitrification point (right). (For interpretation of the references to colour in this figure legend, the reader is referred to the Web version of this article.)

3.2. The effect of printing orientation

The Jacobs working curves, photo-DSC and photo-rheology served as a basis to establish the most convenient exposure time of the MSLA 3D printing experiments, which was set to 15 s (~9.9 mJ cm^{-2}) for the first layer and to 10 s (~6.6 mJ cm^{-2}) for the subsequent layers. Nevertheless, these results gave no clue on the molecular structure and other important parameters such as the printing orientation or the network density which strongly influences the mechanical performance [16]. Two sets of specimens with various curing times were printed in three different directions *x*, *y*, z to investigate the influence of printing orientation on thermomechanical performance (Fig. 5). The first set was measured without post-curing ("green body") while the second one was post-cured for 30 min (~ 18.0 J cm^{-2}). A pronounced effect of the printing layers' orientation relative to the applied force was observed. The classic HDT measurement as well as our modified method applies a constant load to the sample. In addition, a non-isothermal creep occurred at higher temperature, causing a mechanical failure of the specimen at a certain point [29]. The deformation and temperature at break could be used as material characteristics for the specified heating protocol. The latter effectively replaces the time to break which is usually evaluated in isothermal creep tests.

Significant differences in samples' temperature resilience were observed to highly depend on the printing orientation (Fig. 6). Printing in the *x* direction showed the highest resistance to failure due to the non-isothermal creep thanks to the most effective layer alignment in the given load direction. The force was applied in the direction normal to the printed layers; bending the whole layers when applied. A growing crack had to pass through several boundaries formed by layered structure of weak and compact areas before resulting into the ultimate failure of the specimen. On the other hand, specimens printed in the *z*-direction showed lowest thermomechanical resistance to the propagating crack during the deformation at higher temperatures because the weak layer boundaries were aligned with the applied stress. Thus, the adjacent layers were separated by a crack which started at the tensile-deformed side of the sample and grew easily through the weak layer boundary. The printing in the *y*-direction exploited intermediate thermomechanical resistance when compared to *x* and *z* direction (Fig. 6). The possible explanation might be the fact that the propagating crack does not need to cross the interlayer region where it can branch and delaminate the neighbouring layers, thus, dissipating more energy.

The photos of uncured sample printed in different directions after the mechanical stress are shown in (Fig. 7). The distance between layers was measured to be approx. 50 μm as expected according to the set layer thickness of 50 μm. The same layer distribution was observed for all uncured samples printed in *x*, *y* and *z* direction. Uncured samples

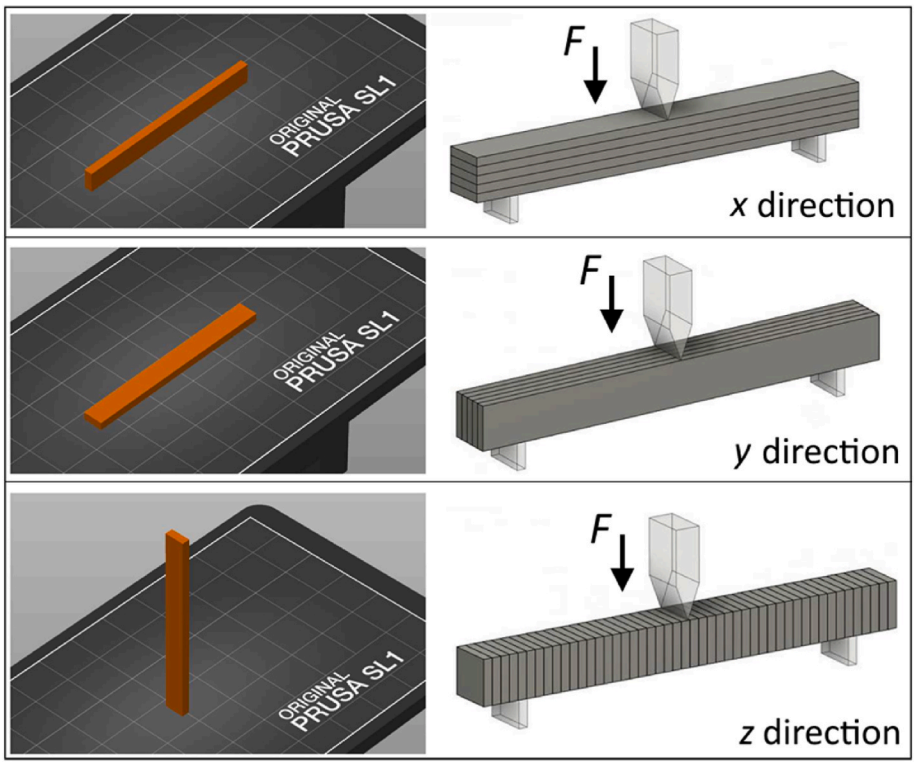

Fig. 5. Schematic representation of the print orientation as the specimens were positioned on the printing plate (left) and in the combined DMA-HDT test with corresponding layer orientation relative to the applied force (right).

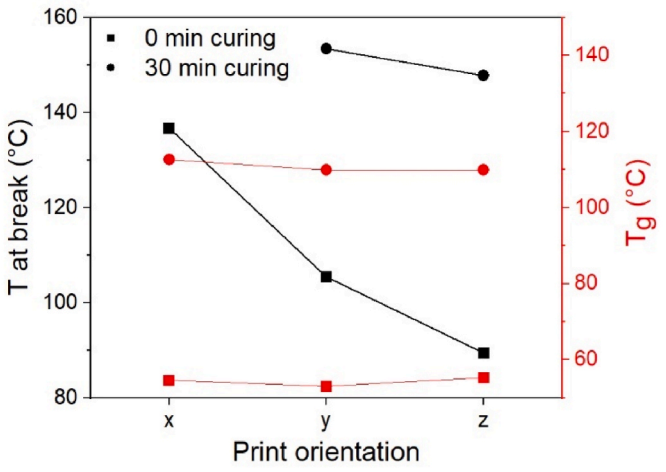

Fig. 6. The influence of print orientation on temperature at break and T_g. The sample with dimensions 48.5 × 5 × 3.5 mm^3 printed in the *x* direction and cured for 30 min did not break until the end of the test. (color in print)

showed the highest concentration of cracks combined with worse thermomechanical performance, i.e., low T at break, polymer network density, HDT, and T_g, caused by the lower interconnection of individual layers and decreased double bond conversion. However, after 30 min post curing the boundaries between the individual layers were not distinguishable anymore. This correlates well with the increased polymer network density and the improved mechanical properties of the material, which is further discussed. An uncured sample after exposure to mechanical stress is shown in Fig. 7 bottom right. The cracks passed through the boundaries between the layers of the sample, as expected. This phenomenon was not observed for none of the cured samples at any print direction.

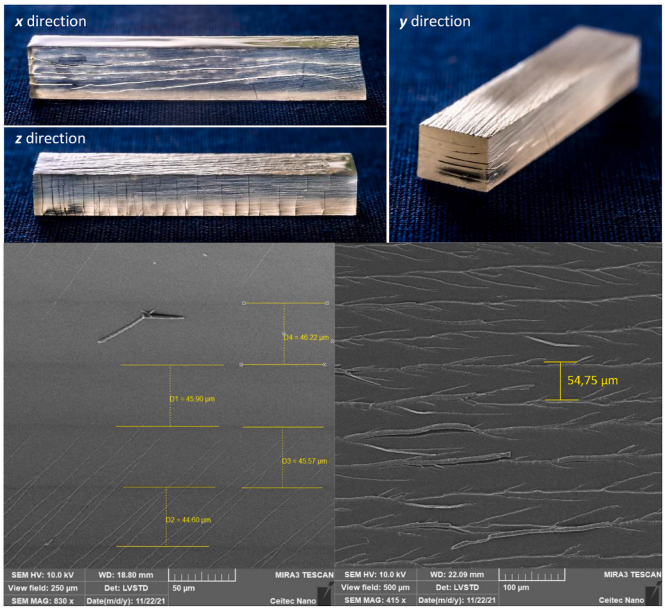

Fig. 7. Uncured samples printed in *x*, *y*, and *z* direction after DMA measurement, revealing print-direction dependent delamination (top); SEM image of an uncured sample showing printed layers as was schematically presented in Fig. 5 with dimensions of approx. 50 µm (bottom left) and a sample after exposure to mechanical stress with cracks passing through the boundaries between the layers (bottom right).

The failure temperature and the mechanical resistance increased significantly after post-curing for all printing orientations due to the stronger interconnection of individual layers because of the increased double bond conversion. These results indicated pronounced improvement of the non-isothermal creep resistance which decreased in the

order $x > y > z$ printing direction. Hence, it would significantly extend the service lifetime of these materials in applications with demands on good mechanical performance, especially at higher temperatures. The glass transition temperature remained the same for all directions as this property was not influenced by the load direction (Fig. 5) and solely depended on the molecular structure within the material regardless the layer orientation and stress transfer between the neighbouring layers or individual voxels. The printing orientation had also a pronounced impact on the temperature at break which differed for the uncured samples. A longer post-curing reduced the difference, as the layers' interconnection was improved, but it was still significant.

The effect of the print direction was also significant for the determination of HDT and Shore D hardness (Fig. 8). A noticeable difference was observed in print directions x and y even at low curing times. The HDT values for x-direction showed better results. The difference in various directions gradually decreased as the material became more and more resistant to deformation. Thus, it is particularly important to consider the loading direction regarding the printing direction for the correct evaluation of thermomechanical properties and HDT. It can be concluded that the combined DMA-HDT analysis can conveniently visualize the mechanical properties varying with the printing layers' orientation respective to the applied force and stress transfer of applied force within the material, while the thermal properties were insensitive to the orientation.

3.3. The effect of post photo-curing time

Both professionals and hobby users often purposely decrease the post-curing time of the printed object to shorten the production time. Moreover, they commonly neglect the requirements for the irradiation of the printed objects from all sides of the printout. These flaws might have serious consequences for the part durability which can be critical if we consider engineering of load bearing applications or applications requiring low or no migration of molecules from and/or into the object. It may also prove critical for various structures with hidden surfaces such as the inner walls of cells and cavities which might be inaccessible to the post-curing light.

The curing time and the total exposure energy had a major influence on the mechanical performance. The temperature dependence of the printed objects' storage modulus and tan δ is shown in Fig. 9 for different post-curing times and exposure doses. The storage modulus is a measure of sample's elastic behaviour associated with its stiffness. We have selected the representative temperature of 35 °C for the precise comparison of the glassy modulus between the samples. This point lay deep in the glassy region of all the tested specimens while the heating cycle has already stabilized after starting the heating procedure at 30 °C. The tan δ can be interpreted as a damping factor reflecting the energy dissipation of the sample at the given temperature. Moreover, the values of G_N^0 , υ_e, M_c, and T_g are also stated in Supplementary data (Table S1).

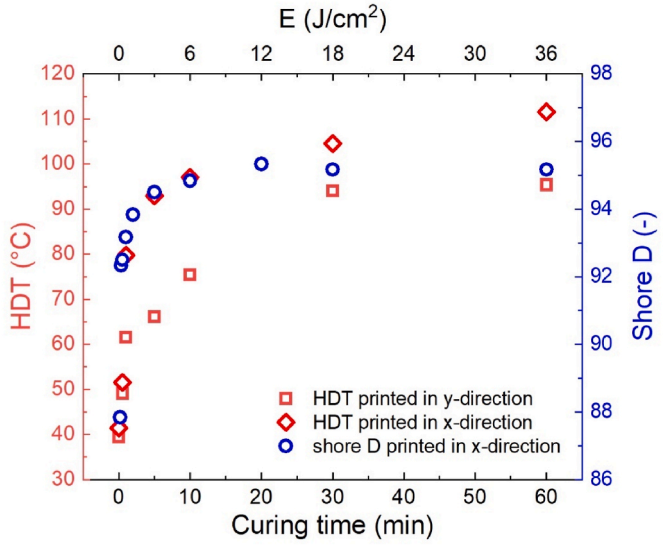

Fig. 8. HDT and as a function of curing time for x and y print orientation combined with shore D hardness of the samples printed in x-direction showing similar trend. The negative influence of the layer orientation towards the applied stress on HDT may be seen.

The prolonged curing time and higher exposure doses led to the significant shift of the T_g and the whole glass transition region towards higher temperatures (Fig. 10). There was also a noticeable increase in G_N^0 at 35 °C which was partially connected to the increased network density, as will be explained later, but also to the higher relative distance from the glass transition due to the increased T_g.

Further information was extracted from the temperature dependence of the flexural deformation induced by the superimposed static stress (Fig. S2). After a short period dominated by the sample's volume expansion, manifested by negative strain values, the deformation started to increase, i.e., bending the testing specimen. That corresponded to the increased segmental motion of the polymer network and softening of the material incurred at the glass transition region. The maximum of the detected deformation shifted to lower values and higher temperatures for the post-cured samples due to the increased network density (Fig. S2). The deformation maximum was followed by the rubber elastic region (Fig. S2).

The polymer network density, evaluated according to eq. (5), increased with the prolonged post-curing time, as expected (Fig. 10). Subsequently, higher exposure doses also led to the increase in all the investigated thermomechanical properties (Table S1) and hardness. The increase in glass transition temperature, HDT and network density was asymptotic, i.e., tending to a limit (Fig. 10). The limit value is supposed to correspond either to the completely cured system or, more precisely, to a fully cured system under the given post-processing conditions determined among others by the light wavelength, exposure dose, and temperature in the curing chamber.

Uncured 3D printing resins contain large free macroradicals unable to react at common temperatures beyond the vitrification point due to the hindered diffusion, which results into imperfect UV curing with a lower conversion. Some materials with low double bond conversion might show problems during the post-curing at higher temperatures, especially when not fully cured, causing the emergence of cracks in the objects (Fig. 7). This is given by inhomogeneous thermal expansion of the object in individual layers where the conversion is a function of the z-coordinate as well as by the non-homogenous distribution of the temperatures at the surface and inner parts of the printed objects. In combination with the extraction of free monomers from the object body and diffusion of a thermally expansive washing solvent, such as isopropanol, it might lead to either formation of small cracks along the layers and/or complete destruction of the printed object, deteriorating the mechanical performance of the material [30]. The diffusion of the free monomers or pending chain ends can be increased by heating the system above its glass transition temperature, bringing about a full reaction of the free radical. Even though the post-curing at elevated temperature was not investigated in this study, a similar phenomenon has been observed during the DMA-HDT measurements. The post cured samples had yellowish colour caused by the light absorption of the free radicals, while the samples after the measurement were colourless (Fig. S3).

Two main trends were observed from the dependence of the thermomechanical properties on the curing time and exposure dose (Fig. 10). Until 5 min curing time, there was an exponential increase in all the studied properties. Further increase was rather linear, approaching a limit value. Two characteristic curing times were established from this behaviour - the minimal curing time (t_{min}) which may be

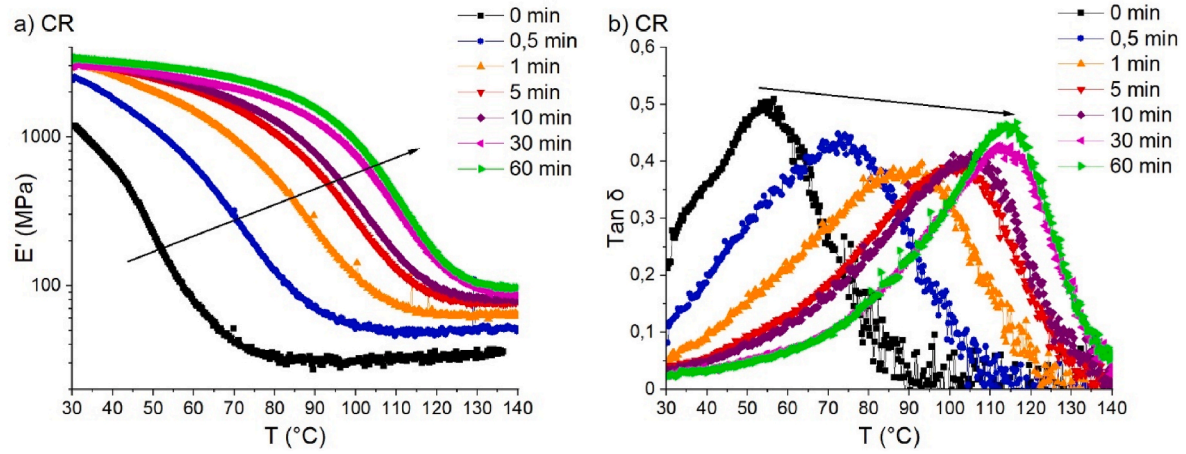

Fig. 9. DMA data for a) storage modulus and b) tan delta as a function of temperature for samples with the dimension of 48.5 × 5 × 3.5 mm^3 cured for 0–60 min. Curve shift caused by the increasing curing time is highlighted with an arrow pointing in the direction from 0 to 60 min.

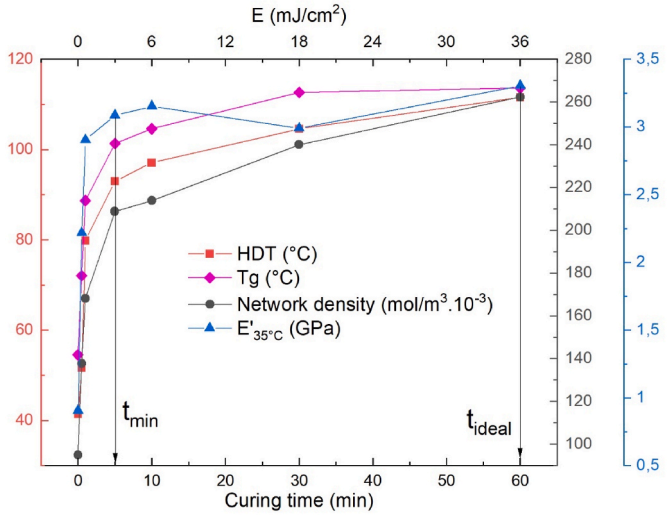

Fig. 10. Graph showing the thermomechanical properties evaluated by the simultaneous DMA-HDT measurement as a function of post-curing time and the exposure energy *E*.

suitable for basic undemanding applications as the initial sharp improvement of all properties was already saturated, while the ideal curing time (t_{ideal}) delivered the maximal thermomechanical properties reachable at the given post-processing conditions. We note that these values are connected to the layer thickness and may differ for thicker or thinner layers. The tested resin reached the limit values after 60 min of curing. This time was considered to be the ideal, since it showed the maximal network density, plateau, deformation, HDT and storage modulus at 35 °C, i.e., the best thermomechanical properties obtained in this study. The minimal post-curing time was set to 5 min (~3.0 J cm^{-2}). We remind the reader that the storage modulus in the rubbery region was the basis for the network density evaluation according to Eq. (5).

The network density (Fig. 11 left) increased with a similar trend as T_g (Fig. 10). The molecular weight between entanglements decreased with the increasing curing time as it is inversely proportional to the network density. The polymer stiffness is dependent on the relative distance to the glass transition temperature as well as on the network density [37]. Thus, the samples with the highest exposure doses were also the least flexible. As far as the maximal deformation is concerned (Fig. 11 left), the dependence on the curing time showed an inverse trend to the other studied parameters (Fig. 8). The temperature dependence on network density for two main studied parameters, T_g and HDT in shown in Fig. 11 right. It can be concluded that the network density is a driving structural parameter for thermomechanical properties of photoresins, excluding

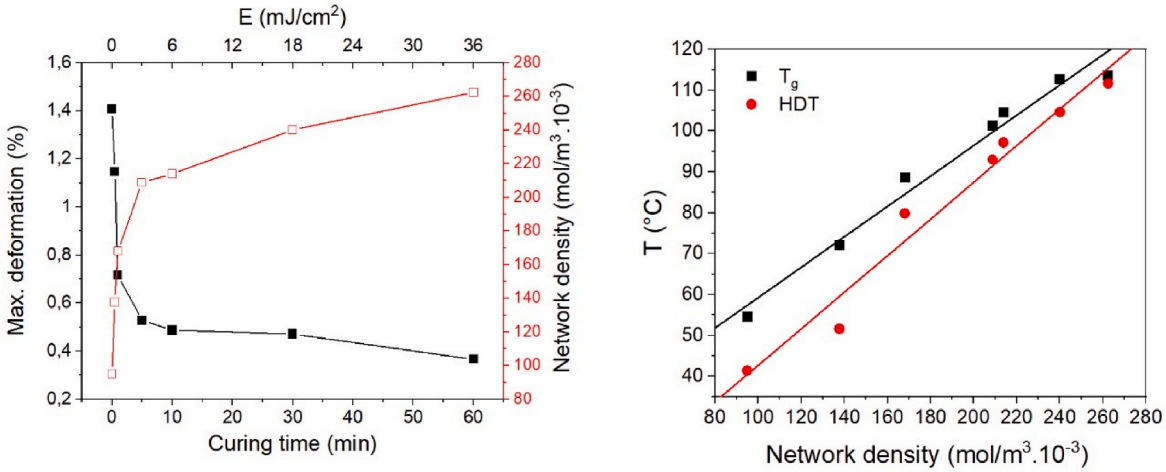

Fig. 11. Network density and maximal deformation as a function of post curing time for sample 48.5 × 5 × 3.5 mm^3 (left) and the temperature dependence on network density for two main studied parameters, T_g and HDT (right).

the influence of molecular structure of the monomer.

The photopolymers used for SLA printing are usually described by thermomechanical and mechanical properties such as tensile/flexural strength, elastic modulus, maximum elongation, HDT, T_g, or hardness, etc. [23,38–40] While some results found in the literature showed a large impact of the printing setup on the mechanical performance [23], other reported effects were far less pronounced [38]. Our results show that all the mechanical and thermomechanical parameters largely depended on the printing setup as well as on the post processing steps but the differences were variable, following the extent of curing and correlating well to a single parameter – the crosslinking density. Previous studies have failed to quantify the crosslinking density as a function related to the specific combination of printing parameters, printed material and cure dose, let alone correlating it to the material performance. This is particularly important when the slow reaction kinetics of the oligomers in the mixed monomer/oligomer UV-curable formulations is considered (Fig. 3) [36]. Thus, we propose to use this property measured at different cure doses as a unification parameter for all UV-curable 3D printing resins to offer a good predictability of mechanical and thermomechanical properties independent of the printing setup. We note that this approach can also capture the changes related to the modification of the resin, e.g. by adding a crosslinker [39].

3.4. Specimen thickness

Furthermore, the dependence of thermomechanical properties on specimen thickness was studied to determine the in-depth post-curing effectivity. This parameter is important to many practical applications but becomes of an utmost importance in complex cellular structures utilizing the cell-size and wall-thickness as tuning parameters of their macroscale performance [5]. Samples with two dimensions fixed at 48.5 × 5 mm^2 and a variable thickness of 5/4.5/4/3.5/3/2.5/2 mm were printed from the tested resin and cured for 1 min. The curing time was chosen in order to observe the largest possible difference; therefore, it was in the range where the properties changed very significantly with the curing time (Figs. 10 and 11). The DMA data showed overlapping curves of storage modulus and tan δ as a function of temperature for different specimen thickness (see Fig. S4). All studied parameters – the deformation, glass transition temperature, molecular weight between entanglements and network density (Fig. 12) remained unaffected by sample thickness. Minor deviations were probably caused by experimental measurement error. This trend was further confirmed by a microscopical FTIR-ATR measurement of double bond concentration (see section 3.5). Thus, the UV light penetrated without significant loss of energy through the sample with thickness between 2 and 5 mm. We note that the standardized testing specimen were 4 mm thick. This might be caused by photobleaching of the TPO pohotoinitiator under the irradiation with light during the post-curing. The light can thus penetrate further to the inner parts of the 3D printed objects and propagate the residual photoinitiator cleavage and curing reaction. However, it is expected that for another photoinitiating system, larger specimen thickness, lower exposure doses, lower light intensities, different light wavelengths with worse match between the curing light emission and photoinitiator absorptivity, or resins filled with particles or light-absorbers, a different effect may be observed and negatively affect the crosslinking during post curing due to the light absorption.

3.5. Double bond conversion

The curing conversion across the specimen thickness was determined using FTIR-ATR spectroscopical microscope (Fig. 13). The C═C double bond absorption bands corresponding to acrylate groups can be seen at 1639 and 1612 cm^{-1} with a twisting vibration at 809 cm^{-1}. The single carbon-carbon bonds (C–C) are visible at 2871 and 2938 cm^{-1} and C–O bonds at 3443 cm^{-1}. The C═O stretching vibration at 1724 cm^{-1} was used as an internal reference for the spectrum normalization. The relative concentration of the C═C and C–C bonds was then calculated as the area under the corresponding peak of the normalized spectra. The results indicated an incomplete conversion of the C═C which correlates with the further change in thermomechanical properties observed at longer exposure times (Fig. 10).

The C═C of acrylate groups undergo a free radical polymerization forming a cross-linked structure. The concentration of the C═C double bonds was studied along the depth of the specimen. “Candy-shell” effect can cause hardening of only a thin outer layer on the sample’s surface upon post curing due to exponential decay of light intensity along the depth of the specimen [27]. Based on this assumption, exponential decay of C═C bonds was expected across the specimen. However, this behaviour was not observed, for the specimen thickness between 2 and 5 mm. The specimen was evenly cured throughout the body already after 1 min of the post curing (Fig. 14) but that was likely connected to the specific combination of parameters in the current experiment

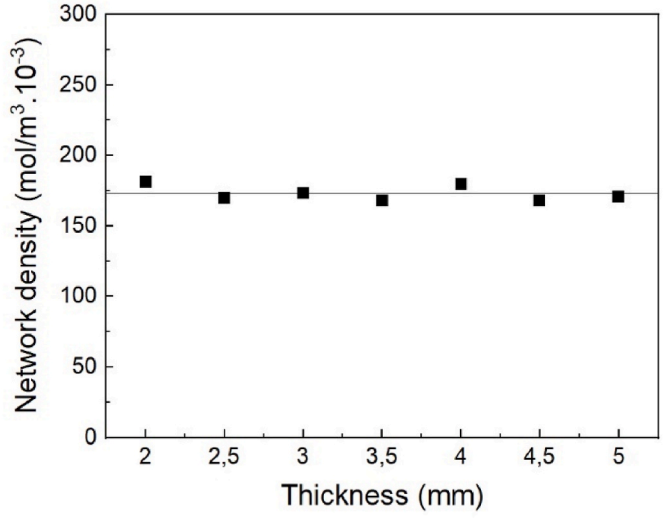

Fig. 12. Network density as a function of specimen thickness for samples post-cured for 1 min. It can be seen, that thickness of the sample between 2 and 5 mm have a negligible effect on network density and consequently on mechanical performance of the resin.

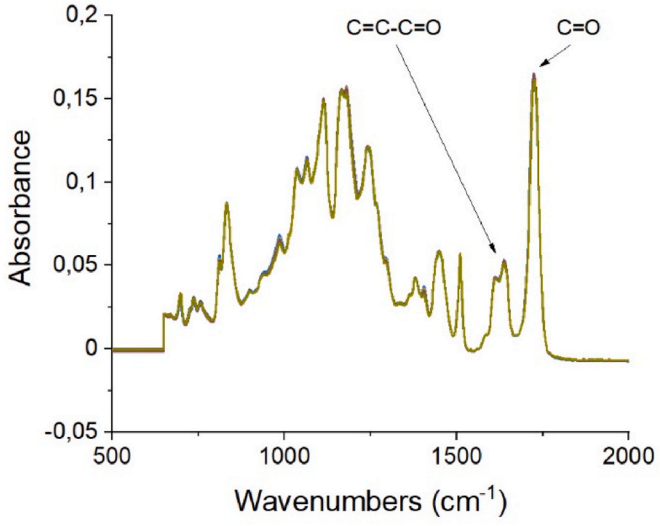

Fig. 13. Overlapped FTIR-ATR spectra of the printed resin post cured for 1 min measured at ten spots evenly distributed across the cross-section of 5 × 5 mm. The spectra confirm the conclusion, that the sample thickness between 2 and 5 mm did not affect the thermomechanical properties.

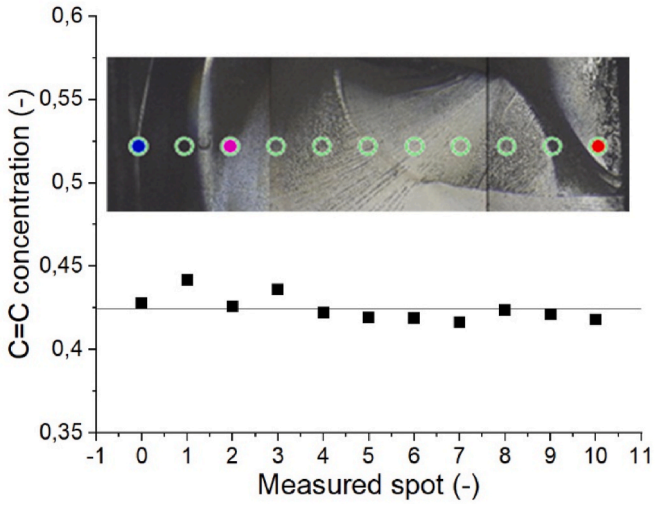

Fig. 14. Graf showing relative concentration of C═C double bonds at 1564-1668 cm^{-1} across the 5 × 5 mm^2 specimen with UV-thermal post curing for 1 min, plotted with constant linear fit line, supplemented with photomicrograph of the measured sample with specific measured spots.

allowing the even penetration of light through the specimen as explained above. The negligible decrease in C═C bond concentration was probably caused by the orientation arrangement in the CW1 curing machine.

The surface of the printed specimens was studied with Confocal Laser Scanning Microscope (CLSM). It was found that all specimens show characteristic square pattern, which occurs before and also after the post treatment. The length of the square side pattern was measured and established to 0.044 mm which corresponded well to the pixels of the SL1 printer LCD panel which was 0.047 mm per pixel. The fact that the surface is structured may support the swelling of solvent during the post-process cleaning. Despite this phenomenon was not systematically investigated, it was observed that the exposure time of the fresh printout to the cleaning in isopropanol had a significant influence on sample appearance and the presence of defects (Fig. S5). A significant effect on thermomechanical properties and final application performance can be expected. Thus, all samples were cleaned for less than 15 s in this study. Nevertheless, the effect of solvent washing on the post-treatment was beyond the scope of the current study even though it is of great importance.

4. Conclusion

A complex characterization method combining the measurement of heat deflection temperature (HDT) and the dynamic mechanical analysis (DMA) was presented to enable a faster characterization of 3D printed photopolymerized systems. In comparison to conventional measurement methods of HDT and DMA, the main advantages of combined technique are faster sample preparation and measurement, lower material consumption, time, energy and capacity savings of the instrument and the ability to compare the results of DMA and HDT for the same sample, while eliminating sample preparation error. Several thermomechanical properties obtained through this method together with auxiliary techniques were used for evaluating the influence of the processing and post-processing parameters such as the post-curing time, specimen thickness, or object orientation on the print platform.

It was concluded that print orientation has large effect on both HDT and temperature at break. The printing in *x* direction yielded the most mechanically resistant arrangement because the applied force was perpendicular to the printed layers and the weak interlayer regions. The combined DMA-HDT analysis showed that the mechanical properties varied with the printing layers' orientation respective to the applied force and stress transfer of applied force within the material, while the thermal properties were insensitive to the orientation. It was proven that higher post-processing exposure doses increased the thermomechanical properties, while having an asymptotic behaviour, i.e. tending to a limit. Same trend, first the exponential increase followed by a slower linear increase, was determined for all the studied material properties (HDT, T_g, E and network density). Two curing times were selected from the measured values as t_{min} suitable for undemanding applications while keeping the process time at minimum and t_{ideal} with the maximum network density and the best thermomechanical performance. The method is expected to be applicable for all photopolymerized as well as thermosetting systems. Furthermore, the thickness of the sample between 2 and 5 mm had in our case a negligible effect on the network density, C═C bonds conversion and consequently on the mechanical performance of the printed structures. However, it is expected that larger thickness, different curing times or presence of particles may negatively affect the crosslinking and thermomechanical properties in deeper layers due to uneven light penetration, especially when the post-curing is applied. It was also observed that washing in isopropanol has large effect on thermomechanical properties due to the swelling resulting into delamination even though it was not systematically studied. All these phenomena possibly relate to the presence of regions at the layer boundaries which are not fully cured due to the hindered propagation of the photoreaction beyond the vitrification point.

Finally, we propose that the presented technique may represent a new single-test standard helping to unify the available technical information on photopolymerized 3D printed bodies, in order to be able to fully predict the material characteristics. The acquired data considering the influence of preparation parameters on thermomechanical properties of final 3D printed product may also significantly help in designing the processing conditions and thus enable proper choice of application field.

Data availability statement

The processed data required to reproduce the above findings are available to download as an electronic supplementary file.

CRediT authorship contribution statement

Martina Štaffová: Conceptualization, Data curation, Investigation, Formal analysis, Writing – original draft, Writing – review & editing. **František Ondreáš:** Conceptualization, Formal analysis, Methodology, Writing – review & editing. **Juraj Svatík:** Data curation, Formal analysis, Investigation. **Marek Zbončák:** Conceptualization, Formal analysis, Validation, Writing – review & editing. **Josef Jančář:** Formal analysis, Supervision. **Petr Lepcio:** Formal analysis, Funding acquisition, Investigation, Methodology, Supervision, Validation, Writing – review & editing.

Declaration of competing interest

The authors declare the following financial interests/personal relationships which may be considered as potential competing interests: Prusa Polymers company conducts commercial activities in the field of 3D printing including manufacturing and selling of 3D printing equipment, materials and consumables. Among others, it has developed and manufactured the SL1 printer and CW curing unit used within the study. - M.Z.

Acknowledgement

Petr Lepcio acknowledges the GF21-43070L project supported by the GA ČR. Martina Štaffová acknowledges the internal student project of the Central European Institute of Technology, Brno University of

Technology [grant number CEITEC VUT-J-20–6317]. Marek Zbončák acknowledges the FW01010650 project supported by the TA ČR. We also acknowledge the CzechNanoLab Research Infrastructure supported by MEYS CR (LM2018110) for providing equipment for microscopical analysis.

Appendix A. Supplementary data

Supplementary data to this article can be found online at https://doi.org/10.1016/j.polymertesting.2022.107499.

References

[1] Tuan D. Ngo, Kashani Alireza, Imbalzano Gabriele, T.Q. Kate, David Hui Nguyen a, Additive manufacturing (3d printing): a review of materials, methods, applications and challenges, Compos. B Eng. 143 (2018) 172–196, https://doi.org/10.1016/j.compositesb.2018.02.012. Issn 13598368. Dostupné z.

[2] Carl G. Schirmeister, Hees Timo, H. Licht a Erik, Rolf Mülhaupt, 3d printing of high density polyethylene by fused filament fabrication, Addit. Manuf. 28 (2019) 152–159, https://doi.org/10.1016/j.addma.2019.05.003. Issn 22148604. Dostupné z.

[3] R. Boros, P. Kannan Rajamani a, J.G. Kovacs, Combination of 3d printing and injection molding: overmolding and overprinting, Express Polym. Lett. 13 (10) (2019) 889–897, https://doi.org/10.3144/expresspolymlett.2019.77. Issn 1788618x. Dostupné z.

[4] Tianyun Yao, Zichen Deng, Kai Zhang, Li Shiman, A method to predict the ultimate tensile strength of 3d printing polylactic acid (Pla) materials with different printing orientations, Compos. B Eng. 163 (2019) 393–402, https://doi.org/10.1016/j.compositesb.2019.01.025. Issn 13598368. Dostupné z.

[5] Juraj Svatík, Lepcio Petr, Ondreáš František, Zárybnická Klára, Zbončák Marek, Josef Jančář Přemysl Menčík a, Pla toughening via bamboo-inspired 3d printed structural design, Polym. Test. 104 (2021), https://doi.org/10.1016/j.polymertesting.2021.107405, 01429418. Dostupné z.

[6] Charles W. Hull, Apparatus for Production of Three-Dimensional Objects by Stereolithography, Us4575330a. Uděleno, 1984.

[7] Ligon Samuel Clark, Liska Robert, Stampfl Jürgen, Matthias Gurr a Rolf Mülhaupt, Polymers for 3d printing and customized additive manufacturing, Chem. Rev. 117 (15) (2017) 10212–10290, https://doi.org/10.1021/acs.chemrev.7b00074. Issn 0009-2665. Dostupné z: doi:.

[8] Aydin Sadeqi, Nejad Hojatollah Rezaei, E. Rachel, Owyeung a sameer sonkusale, Three dimensional printing of metamaterial embedded geometrical optics (Mego) 5 (1) (2019), https://doi.org/10.1038/s41378-019-0053-6, 2055-7434. Dostupné z.

[9] Zeyu Chen, Song Xuan, Lei Liwen, et al., 3d printing of piezoelectric element for energy focusing and ultrasonic sensing, Nano Energy 27 (2016) 78–86, https://doi.org/10.1016/j.nanoen.2016.06.048. Issn 22112855. Dostupné z.

[10] Brett E. Kelly, Indrasen Bhattacharya, Heidari Hossein, Shusteff Maxim, M. Christopher, K. Taylor Spadaccini a Hayden, Volumetric additive manufacturing via tomographic reconstruction, Science 363 (6431) (2019) 1075–1079, https://doi.org/10.1126/science.aau7114. Issn 0036-8075. Dostupné z.

[11] Xiaoyan Xu, Awad Atheer, Pamela Robles-Martinez, Gaisford Simon, W. Alvaro Goyanes a Abdul, Basit. Vat photopolymerization 3d printing for advanced drug delivery and medical device applications, J. Contr. Release 329 (2021) 743–757, https://doi.org/10.1016/j.jconrel.2020.10.008. Issn 01683659. Dostupné z: doi:.

[12] Sophia N. Economidou, Dimitrios A. Lamprou a Dennis Douroumis, 3d printing applications for transdermal drug delivery, Int. J. Pharm. 544 (2) (2018) 415–424, https://doi.org/10.1016/j.ijpharm.2018.01.031. Issn 03785173. Dostupné z: doi:.

[13] Bloomquist, J. Cameron, Michael B. Mecham, Mark D. Paradzinsky, et al., Controlling release from 3d printed medical devices using Clip and drug-loaded liquid resins, J. Contr. Release 278 (2018) 9–23, https://doi.org/10.1016/j.jconrel.2018.03.026. Issn 01683659. Dostupné z.

[14] Pant, Prabhat. Residual stress distributions in additively manufactured parts: effect of build orientation. Dostupné z: doi:10.3384/lic.diva-164108.

[15] Yuxuan Wang, Yonghui Zhou, Lin Lanying, Jorge Corker a Mizi Fan, Overview of 3d additive manufacturing (Am) and corresponding Am composites, Compos. Appl. Sci. Manuf. 139 (2020), https://doi.org/10.1016/j.compositesa.2020.106114. Issn 1359835x. Dostupné z.

[16] C. Hofstetter, S. Orman, S. Baudis, J. Stampfl, Combining cure depth and cure degree, a new way to fully characterize novel photopolymers, Addit. Manuf. 24 (2018) 166–172, https://doi.org/10.1016/j.addma.2018.09.025. Issn 22148604. Dostupné z.

[17] Chunguang Li, Jue Cheng, Wenkai Chang, Nie Jun, Photopolymerization kinetics and properties of a trifunctional epoxy acrylate, Des. Monomers Polym. 16 (3) (2012) 274–282, https://doi.org/10.1080/15685551.2012.747143. Issn 1568-5551. Dostupné z.

[18] Young-Jun Park, Lim Dong-Hyuk, Kim Hyun-Joong, Park a Dae-Soon, Sung Ick-Kyung, Uv- and thermal-curing behaviors of dual-curable adhesives based on epoxy acrylate oligomers, Int. J. Adhesion Adhes. 29 (7) (2009) 710–717, https://doi.org/10.1016/j.ijadhadh.2009.02.001. Issn 01437496. Dostupné z: doi:.

[19] Stansbury Jeffrey, W. a Mike, J. Idacavage, 3d printing with polymers: challenges among expanding options and opportunities, Dent. Mater. 32 (1) (2016) 54–64, https://doi.org/10.1016/j.dental.2015.09.018. Issn 01095641. Dostupné z:.

[20] Oropallo William, Les A. Piegl, Ten challenges in 3d printing, Eng. Comput. 32 (1) (2016) 135–148, https://doi.org/10.1007/s00366-015-0407-0. Issn 0177-0667. Dostupné z.

[21] Ali a Bagheri, Jianyong Jin, Photopolymerization in 3d printing, Acs Applied Polymer Materials 1 (4) (2019) 593–611, https://doi.org/10.1021/acsapm.8b00165. Issn 2637-6105. Dostupné z.

[22] Wiktoria Tomal, Krok Dominika, Chachaj-Brekiesz Anna, Lepcio Petr, Ortyl Joanna, Harnessing light to create functional, three-dimensional polymeric materials: multitasking initiation systems as the critical key to success, Addit. Manuf. 48 (2021), https://doi.org/10.1016/j.addma.2021.102447. Issn 22148604. Dostupné z.

[23] Hong, Yong Sung, Kim Ye Chan, Mei Wang, et al., Experimental investigation of mechanical properties of Uv-Curable 3d printing materials, Polymer 145 (2018) 88–94, https://doi.org/10.1016/j.polymer.2018.04.067. Issn 00323861. Dostupné z.

[24] Jaroslaw Kotlinski, Mechanical properties of commercial rapid prototyping materials, Rapid Prototyp. J. 20 (6) (2014) 499–510, https://doi.org/10.1108/Rpj-06-2012-0052. Issn 1355-2546. Dostupné z.

[25] Kim Ye Chan, Hong Sungyong, Hanna Sun, et al., Uv-curing kinetics and performance development of in situ curable 3d printing materials, Eur. Polym. J. 93 (2017) 140–147, https://doi.org/10.1016/j.eurpolymj.2017.05.041. Issn 00143057. Dostupné z: doi.

[26] Yi Gao, Xu Lei, Zhao Yang, Zhengwei You a Qingbao Guan, 3d printing preview for stereo-lithography based on photopolymerization kinetic models, Bioactive Materials 5 (4) (2020) 798–807, https://doi.org/10.1016/j.bioactmat.2020.05.006. Issn 2452199x. Dostupné z.

[27] Uzcategui Asais Camila, Archish Muralidharan, Virginia L. Ferguson, J. Stephanie, Bryant a Robert R. Mcleod, Understanding and improving mechanical properties in 3d printed parts using a dual-cure acrylate-based resin for stereolithography, Adv. Eng. Mater. 20 (12) (2018), https://doi.org/10.1002/adem.201800876. Issn 14381656. Dostupné z.

[28] Mendes Felipe, David Patrocinio Cristian, José M. Laza, Leire Ruiz-Rubio, José Luis Vilas-Vilela, Evaluation of postcuring process on the thermal and mechanical properties of the Clear02™ resin used in stereolithography, Polym. Test. 72 (2018) 115–121, https://doi.org/10.1016/j.polymertesting.2018.10.018. Issn 01429418. Dostupné z: doi:.

[29] Ondreas Frantisek, Jancar Josef, Temperature, frequency, and small static stress dependence of the molecular mobility in deformed amorphous polymers near their glass transition, Macromolecules 48 (13) (2015) 4702–4716, https://doi.org/10.1021/acs.macromol.5b00550. Issn 0024-9297. Dostupné z: doi:.

[30] Alexander Bardelcik, Yang Steven, Faraz Alderson, a Andrew Gadsden, The effect of wash treatment on the mechanical properties and energy absorption potential of a 3d printed polymethyl methacrylate (Pmma), Mater. Today Commun. 26 (2021), https://doi.org/10.1016/j.mtcomm.2020.101728. Issn 23524928. Dostupné z.

[31] Sultan Aati, Akram Zohaib, Barsha Shrestha, Patel Jainish, Shih Benjamin, Shearston Kate, Ngo a Hien, Amr Fawzy, Effect of post-curing light exposure time on the physico–mechanical properties and cytotoxicity of 3d-printed denture base material, Dent. Mater. (2021), https://doi.org/10.1016/j.dental.2021.10.011. Issn 01095641. Dostupné z.

[32] I. Gibson, D. Rosen, B. Stucker, Additive Manufacturing Technologies: 3d Printing, Rapid Prototyping, and Direct Digital Manufacturing, second ed., Springer, New York, 2015, ISBN 978-1-4939-2112-6.

[33] Benjamin D. Fairbanks, F. Timothy, Christopher J. Kloxin Scott, S. Kristi, N. Anseth a Christopher, Thiol−Yne Bowman, Photopolymerizations: novel mechanism, kinetics, and step-growth formation of highly cross-linked networks, Macromolecules 42 (1) (2009) 211–217, https://doi.org/10.1021/ma801903w. Issn 0024-9297. Dostupné z.

[34] Melick Van, H.G.H.L.E. Govaert, H.E.H. Meijer, On the origin of strain hardening in glassy polymers, Polymer 44 (8) (2003) 2493–2502, https://doi.org/10.1016/S0032-3861(03)00112-5. Issn 00323861. Dostupné z.

[35] Xiangquan Wu, Lian Qin, Li a Dichen, Zhongmin Jin, Tilting separation analysis of bottom-up mask projection stereolithography based on cohesive zone model, J. Mater. Process. Technol. 243 (2017) 184–196, https://doi.org/10.1016/j.jmatprotec.2016.12.016. Issn 09240136. Dostupné z: doi:.

[36] J. Jancar, W. Wang, A.T. Dibenedetto, On the heterogeneous structure of thermally cured bis-Gma/Tegdma resins, J. Mater. Sci. Mater. Med. 11 (11) (2000) 675–682, https://doi.org/10.1023/A:1008999023271. Issn 09574530. Dostupné z:.

[37] D.K. Chattopadhyay, Siva Sankar Panda, K.V.S.N. Raju, Thermal and mechanical properties of epoxy acrylate/methacrylates Uv cured coatings, Prog. Org. Coating 54 (1) (2005) 10–19, https://doi.org/10.1016/j.porgcoat.2004.12.007. Issn 03009440. Dostupné z: doi:.

[38] Cosmi Francesca, Dal Maso Alberto, A mechanical characterization of Sla 3d-printed specimens for low-budget applications, Mater. Today Proc. 32 (2020) 194–201, https://doi.org/10.1016/j.matpr.2020.04.602. Issn 22147853. Dostupné z: doi:.

[39] Joseph Borrello, Nasser Philip, C. James, Iatridis a Kevin D. Costa, 3d printing a mechanically-tunable acrylate resin on a commercial Dlp-Sla printer, Addit. Manuf. 23 (2018) 374–380, https://doi.org/10.1016/j.addma.2018.08.019. Issn 22148604. Dostupné z.

[40] Dohyun Kim, Shim Ji-Suk, Lee Dasun, Shin Seung-Ho, Nam Na-Eun, Park Kyu-Hyung, June-Sung Shim, Kim Jong-Eun, Effects of post-curing time on the mechanical and color properties of three-dimensional printed crown and bridge materials, Polymers 12 (11) (2020), https://doi.org/10.3390/polym12112762. Issn 2073-4360. Dostupné z.